Eur. Phys. J. A **7**, 293–298 (2000)

THE EUROPEAN PHYSICAL JOURNAL A

On the Absorption of antibaryons in nuclei

M. Gonin[a], O. Hansen

Niels Bohr Institute for Astronomy, Physics and Geophysics, University of Copenhagen, 2100 Copenhagen, Denmark

Received: 15 July 1999 / Revised version: 10 November 1999
Communicated by P. Kienle

Abstract. Antiproton ($\bar{p}$) and antilambda ($\bar{\Lambda}$) production has been measured for minimum bias in p+A collisions and central A_1+A_2 collisions at the CERN-SPS by the collaborations NA35/49 and NA44. The measurements are extrapolated from rapidity distributions to absolute minimum bias cross sections. It is shown that the $\bar{p}$ cross sections divided by $A_1 \cdot A_2$ follow an exponential trend as a function of a characteristic length obtained from a Glauber type absorption model, while the $\bar{\Lambda}$ cross sections divided by $A_1 \cdot A_2$ are constant. The exponential trend also holds for $\bar{p}$ production at the lower energies of the Brookhaven AGS. A discussion of the physics interpretation of the established trends in terms of an effective absorption cross section is presented.

PACS. 25.75.-q Relativistic heavy-ion collisions – 25.75.Dw Particle and resonance production

1 Introduction

The production of anti-baryons in high energy p+A and A_1+A_2 collisions is of interest because mechanisms different from those in p+p collisions may come into play and because absorption in the hot and dense nuclear medium is of importance (see e.g. [1–3]). This paper presents an analysis of empirical p+A$\rightarrow \bar{p}(\bar{\Lambda})$ and A_1+$A_2 \rightarrow \bar{p}(\bar{\Lambda})$ cross sections with the purpose of establishing global trends as function of (A_1,A_2). The inspiration comes from the successful demonstration of such global trends for the p+A$\rightarrow$J/Ψ and A_1+A_2 $\rightarrow$J/Ψ cross sections in terms of a simple Glauber type absorption model [4,5]. In the J/Ψ case, with one exception, all the measured minimum bias total reduced cross sections follow a single exponential trend as function of a characteristic length, L, derived from the absorption model; the term "reduced cross section" stands for the cross section divided by $A_1 \cdot A_2$. The exception from this trend in the J/Ψ case occurs for non-peripheral Pb+Pb collisions.

It is demonstrated in the present paper that the $\bar{p}$ reduced cross sections also follow exponentials as a function of L, while the $\bar{\Lambda}$ reduced cross sections are constant with L. It is further shown that this implies a simple dependence with A_1,A_2.

In Sect. 2 the recipe for deriving the characteristic length L from the absorption model is described and the A_1,A_2 dependence of L is established. Section 3 presents the empirical results as well as the somewhat intricate procedure for extrapolating the data to a uniform body of total minimum bias cross sections. In Sects. 4 and 5 the global trends are established and Sect. 6 deals with the physics interpretation of the demonstrated systematics and in particular with the problem of the use of a Glauber type recipe which is not clearly *a priori* justifiable.

2 Calculation of L

The absorption lengths, L used in the analysis of J/Ψ production are derived from a Glauber type statistical absorption model, see e.g. [6,7], for p+A processes. In the model the projectile and the created rare particle move forward in straight line trajectories. The rare particle (X) is created at a well defined location z' along the incoming projectile direction inside the target nucleus and undergoes absorption on its forward trajectory out through the target nucleus with an absorption cross section σ. The probability distribution of the creation location z' through the nucleus is assumed to be uniform.

After integration over z' the formulae for total minimum bias p+A cross sections [7] are

$$\frac{\sigma(p+A\rightarrow X)}{A\sigma(p+p\rightarrow X)} = \exp(-L_{pA}/\lambda) =$$

$$\frac{1}{(A-1)\sigma}\int d\boldsymbol{b}(1-\exp(-L_{pA}(b)/\lambda)), \quad (1)$$

where

$$L_{pA}(b)/\lambda = \int_{-\infty}^{\infty} dz(A-1)\sigma\rho(\boldsymbol{b},z) \quad (2)$$

[a] Also at Ecole Polytechnique, L.P.N.H.E., 91128 Palaiseau, France

and

$$1/\lambda = \sigma\rho_0 = \sigma/(\frac{4\pi}{3}r_0^3). \quad (3)$$

$\boldsymbol{b}$ is the transversal position of the incoming proton relative to the center of nucleus A, expressed by the impact parameter $b = \mid \boldsymbol{b} \mid$ and the azimuthal angle; z is the coordinate along the the incoming direction and the integrations are over all space and $\rho(\boldsymbol{b}, z)$ is the nuclear density distribution normalized to unity when integrated over all space. A is the baryon number of the target nucleus and X is absorbed with a cross section σ, which is assumed independent of $\boldsymbol{b}$ and z. The r_0 is chosen to be 1.1198 fm, so that ρ_0=0.17 nucleons per fm^3.

For A_1+A_2 collisions the absorption length L satisfies [7]

$$\frac{\sigma(A_1 + A_2 \to X)}{A_1 A_2 \sigma(p + p \to X)} =$$

$$\exp(-L_{A_1A_2}/\lambda) = \exp(-(L_{pA_1} + L_{pA_2})/\lambda), \quad (4)$$

where $\sigma(A_1 + A_2 \to X)/(A_1A_2)$ is the reduced cross section. The density distribution $\rho(\boldsymbol{b}, z)$ is either of Saxon-Woods shape or is a uniform spherical density distribution. The Saxon-Woods shape is

$$\rho(\boldsymbol{b}, z) = \frac{1}{V_A}\frac{1}{1 + \exp((\sqrt{b^2 + z^2} - R_A)/a)}, \quad (5)$$

with V_A denoting the volume of nucleus A, a=0.51 fm and R_A is adjusted to give an average density of 0.17 nucleons/fm^3 (or equivalently $V_A = \frac{4\pi}{3}r_0^3A$). If the uniform distribution is used the density is also fixed at 0.17 nucleons/fm^3. $L_{A_1+A_2}$ is calculated from the above formulae by numerical integration for a chosen value of σ.

For $\sigma \to 0$ an expansion of the righthand part of (1) in L_{pA}/λ to first order and in $L_{pA}(b)/\lambda$ to second order gives

$$L(\sigma \to 0) = \frac{\rho_0}{2(A-1)}\int d\boldsymbol{b}L^2(b). \quad (6)$$

The L-value becomes independent of σ and for the uniform spherical distribution

$$L_{HS}^0 = \frac{3}{4}\frac{A-1}{A}R, \quad (7)$$

where R is the radius of the spherical distribution $R = r_0A^{\frac{1}{3}}$.

Table 1 lists a selection of L-values calculated for each A_1,A_2 combination both for a homogeneous spherical density distribution in the limit of no absorption and for a Saxon-Woods distribution with a finite absorption of σ=2.14 fm^2. With the exception of the p+Be case, the ratio $L_{HS}^0/L_{SW}^{2.14}$ is constant to better than 1%, so one can write with this accuracy, by use of (4) and (7),

$$L_{SW}^{2.14} = 0.515(\frac{A_1 - 1}{A_1}A_1^{\frac{1}{3}} + \frac{A_2 - 1}{A_2}A_2^{\frac{1}{3}}). \quad (8)$$

The L-values thus to good accuracy have a simple mass dependence, except for the lightest system.

L-values can also be calculated for cross sections corresponding to collisions of finite centrality. In such cases (4) is not valid, i.e. the additivity of the p+A L-values does not hold. Also the integrations have higher dimensions and the simple mass dependence of (8) will not hold. In order to preserve the simplicity of the model for total minimum bias cross sections, we have chosen to extrapolate the data, rather than to calculate L-values corresponding to the experimental centrality conditions.

3 Data extrapolations and systematic uncertainties

The data consist mainly of multiplicities per unit rapidity (dn/dy) near midrapidity and they are quoted in tables 1, 2 and 3 in the next two sections. In many cases part of a dn/dy distribution has been measured, in some cases there is only a value at midrapidity. The p+A data have in all cases been obtained with a trigger condition that is close to a minimum bias condition, whereas all the heavy ion data are from central triggers. The experimental results must therefore be extrapolated in rapidity and from a centrality condition to a minimum bias condition in order to be compared to the absorption model as explained above. The experimental cross sections are evaluated by

$$\sigma(A_1 + A_2 \to X) = (dn/dy)F_1(y)F_2(b)F_3\sigma_{inel}, \quad (9)$$

where σ_{inel} stands for the total geometrical cross section in fm^2 parametrized as

$$\sigma_{inel} = 6.86(A_1^{1/3} + A_2^{1/3} - 1.32)^2. \quad (10)$$

The extrapolations F_1 and F_2 have been calculated by means of the event generator RQMD [8]; F_3 is used only for AGS data where $\bar{\Lambda}$ decays may contribute to the $\bar{p}$ yield (see Sect. 5). The choice of the RQMD event generator was made because the model generally gives a good acount of measured dn/dy-distributons and of the dependence on centrality. Any other model with similar characteristics could have been used.

The F_1 correction is calculated as the ratio between the RQMD total multiplicity and the RQMD midrapidity dn/dy value for particle X. The shapes of the RQMD dn/dy distributions agree well with the observed shapes for the rapidity intervals covered by experiment and the correction, by construction, is independent of the absolute RQMD multiplicity. The experimental trigger condition was simulated by a cut on the impact parameter b, such that the RQMD ratio between central cross section and inelastic cross section equalled the experimentally quoted ratio, typically near 5%, 7% or 10% for heavy ion collisions. The F_2 extrapolation is the ratio of the RQMD integrated dn/dy for particle X in the minimum bias cut and in the central cut on impact parameters.

The uncertainties given in the tables in the column for the reduced cross sections only reflect the experimental

Table 1. Antiproton results from CERN-SPS

System	L^0_{HS}	$L^{2.14}_{SW}$	σ_{inel}	y	dn/dy	F_1	F_2	$\sigma/(A_1A_2)$	Ref.
p+S	2.58	1.60	56	3.0	0.032	2.60	1.00	0.146±0.015	[11]
p+Au	4.86	2.96	208	3.0	0.046	2.60	1.00	0.126±0.014	[11]
S+S	5.17	3.20	174	3.5	0.40	3.10	0.36	0.076±0.019	[11]
S+Ag	6.55	4.08	301	3.5	0.60	3.10	0.37	0.060±0.021	[11]
S+Au	7.45	4.56	405	3.5	0.70	3.10	0.39	0.055±0.016	[11]
Pb+Pb	9.90	6.01	763	3.0	2.40	2.60	0.34	0.037±0.008	[12]
p+Be	1.55	0.84	21	2.7	0.045	2.80	1.00	0.294±0.070	[13]
p+S	2.58	1.60	56	2.7	0.047	2.80	1.00	0.230±0.060	[13]
p+Pb	4.95	3.01	216	2.7	0.062	2.80	1.00	0.180±0.040	[13]
S+S	5.17	3.20	174	2.7	0.65	2.80	0.36	0.112±0.022	[13]
S+Pb	7.54	4.60	416	2.7	0.92	2.80	0.39	0.063±0.012	[13]
Pb+Pb	9.90	6.01	763	2.7	1.80	2.80	0.34	0.031±0.010	[14]

Lengths are in fm and cross sections in fm^2. The absorption lengths L are defined in (4), and the factors F in (6). The Pb+Pb dn/dy has not been rescaled to a beam momentum of 200 GeV/c.

uncertainties on the dn/dy measurements. The extrapolations F_1 and F_2 both carry statistical and systematic uncertainties. The statistical uncertainties stem from the finite number of events calculated and are kept small compared to the uncertainties of the measurements. The systematic uncertainties on F_1 originate from RQMD predicted dn/dy versus y distributions that do not agree with the true dn/dy distributions. In the four cases for $\bar{\Lambda}$ measurements, where part of a dn/dy distribution has been measured, the RQMD predictions do agree quite well with the data. Uncertainties on the order 10% are a realistic estimate for the absolute value for F_1. Note that the absolute multiplicity values are not relevant for this study, only the relative changes from one (A_1,A_2) combination to another are. The correction factor F_2 is due in first order to the geometry of the collision as can be seen from the tables and therefore small uncertainties are expected. Some experimental checks for F_2 are possible for $\bar{p}$ using the BNL-AGS data. The E-802 collaboration has reported for Si+Al, Si+Au [9] and Au+Au [10] dn/dy values for both central and minimum bias triggers. From these data we found the following values for F_2: 0.45 ± 0.14 for Si+Al, 0.42 ± 0.10 for Si+Au and 0.46 ± 0.10 for Au+Au. These values can be compared with the RQMD F_2 values listed in the tables: 0.35 for Si+Al, 0.37 for Si+Au and 0.40 for Au+Au. As can be seen the agreement is reasonable and the fact that the measured values are systematically higher than the RQMD values suggest that the experimental minimum bias data may not correspond to exactly 100% of σ_{inel} but rather to some large fraction of σ_{inel} because of threshold effects in the detectors.

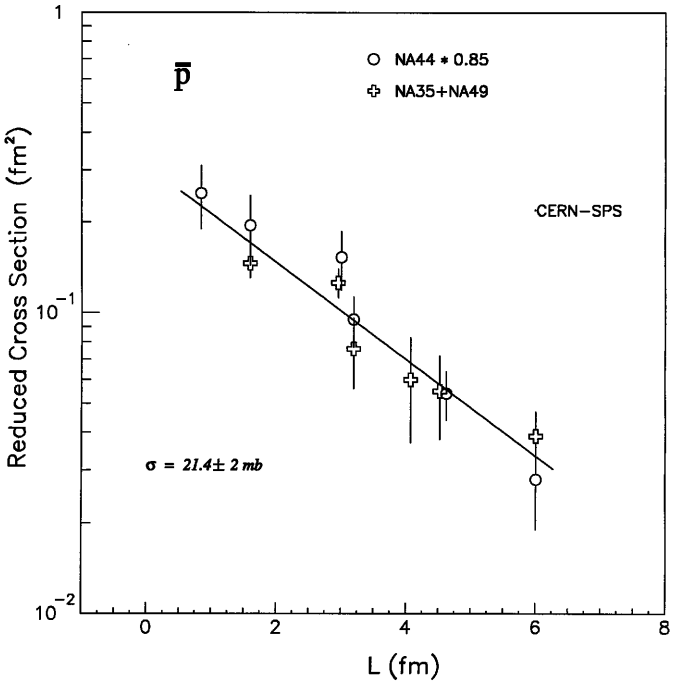

Fig. 1. Reduced cross sections for $\bar{p}$ measured at CERN-SPS. The line represents the simultaneous fit to the data. The Pb+Pb data obtained at 158 GeV are rescaled to 200 GeV by 1.06

4 CERN-SPS results

The A_1+A_2 → $\bar{p}$ data are collected in Table 1 together with references to the appropriate experiments. The absorption lengths L carry a superscript that gives the absorption cross section used in the integrations (1) in units of fm^2. The subscript SW indicates that the Saxon-Woods geometry (5) was used, while HS stands for a homogeneous spherical density distribution with a sharp edge. The $\bar{\Lambda}$ results are collected in Table 2. Figures 1 and 2 show the reduced cross sections plotted versus $L_{A_1A_2}$. The L-scale depends on the absorption cross section, and the scale for $\bar{p}$ production is the result of an iterative process. The criterion for the iteration was that the cross section assumed for L agrees with the slope of the exponential through the data. The $\bar{\Lambda}$ results in Fig. 2 do not exhibit a slope and the L-values were calculated for σ=0.

Table 2. Antilambda results from CERN-SPS

System	L^0_{SW}	σ_{inel}	y	dn/dy	F_1	F_2	$\sigma/(A_1A_2)$	Ref.
p+S	1.99	56	1.75-4.75	0.015	2.50	1.00	0.066±0.013	[11]
p+Au	4.40	208	1.25-4.75	0.015	2.50	1.00	0.040±0.013	[11]
S+S	3.99	174	1.25-4.75	0.91	2.50	0.30	0.116±0.032	[11]
S+Au	6.40	405	3.25-4.75	0.92	3.20	0.33	0.062±0.012	[11]
Pb+Pb	8.99	763	3.0	5.00	2.50	0.30	0.066±0.014	[15]

Units and definitions are as in Table 1. Pb+Pb was not rescaled.

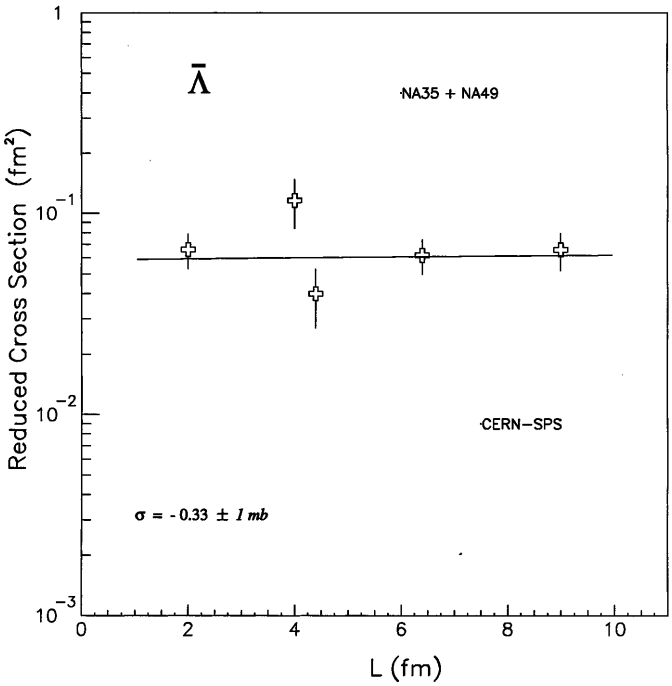

Fig. 2. Reduced cross sections for $\bar{\Lambda}$ measured at CERN-SPS. The line represents an exponential fit to the data. The Pb+Pb data obtained at 158 GeV are rescaled to 200 GeV by 1.07

The reduced $\bar{p}$ cross sections from NA44 and NA35/49 data do not agree in absolute values, but they exhibit nearly identical slopes with L. The data from NA44 as presented in Fig. 1 were (arbitrarily) rescaled by 0.85. The slope value from the fit of Fig. 1 is σ= 21.4 ± 2 mb and is in agreement with separate fits to the data from each experiment.

The beam momentum per nucleon for Pb is lower than for protons and S. The Pb beam data in Fig. 1 (but not in the table) have been corrected upwards by 6% to correspond to the S and p beam conditions. The correction was derived from the RQMD model. No correction was applied for the $\bar{\Lambda}$ results in Fig. 2 for Pb because of the large statistical uncertainties on the data.

The most conspicuous result of the present analysis is that all reduced cross sections for $\bar{p}$ production fall on a single exponential curve (χ^2/dof = 1.07). The second qualitative result is the lack of a break in the exponential for Pb+Pb→ $\bar{p}$, in contrast with the observation for J/ψ production [5], where the Pb+Pb result for minimum bias conditions fall below the global exponential trend. For J/ψ the deviation from the global exponential increases with increasing centrality; it is unfortunately not possible to analyse $\bar{p}$ production for Pb+Pb as a function of centrality due to the lack of data.

As can be seen from Fig. 2, the $\bar{\Lambda}$ reduced cross sections are constant as a function of L. The value for σ obtained from the fit is consistent with zero.

Finally, from p+Be up to Pb+Pb collisions for $\bar{p}$ and from p+S up to Pb+Pb collisions for $\bar{\Lambda}$, the results can be summarized as

$$\sigma(A_1 + A_2 \rightarrow \bar{p}) \propto (A_1 \cdot A_2) \exp(-\rho_0 L_{A_1+A_2}\sigma) \qquad (11)$$

and

$$\sigma(A_1 + A_2 \rightarrow \bar{\Lambda}) \propto (A_1 \cdot A_2) \qquad (12)$$

where the result of (12) is in fact model independent.

5 BNL-AGS results

The A_1+$A_2 \rightarrow \bar{p}$ data obtained at the lower beam momentum (14.6 GeV/c) are collected in Table 3 together with references to the appropriate experiments. Relevant results concerning $\bar{\Lambda}$ are not available at AGS energies. The $\bar{p}$ data obtained at the AGS are contaminated by antiprotons from the decay of $\bar{\Lambda}$. An estimate [18] for the E802 experiment shows that about 50% of the antiprotons from $\bar{\Lambda}$-decays are identified as antiprotons. In order to correct for this contamination, the $\bar{\Lambda}$ rates were estimated from the p+p result of $\bar{\Lambda}/\bar{p} = 0.20 \pm 0.04$ and the p+p→ $\bar{p}$ yield measured at 19 GeV/c [17]. The $\bar{\Lambda}$ cross section was first extrapolated from 19 GeV/c to the AGS heavy ion momentum of 14.6 GeV/c with the RQMD model, an extrapolation that agrees with the empirical p+p systematics [19]. Next it was assumed that (12) holds at AGS energies for $\bar{\Lambda}$ production and a $\bar{\Lambda}$ cross section could then be constructed for each A_1,A_2 combination and an F_3 correction could be deduced. The F_3 corrections from this procedure are shown in Table 3.

The F_3 corrections leads to a $\bar{\Lambda}/\bar{p}$ ratio near one for Au+Au minimum bias collisions in qualitative agreement with the measured values for central Au+Pb reactions [20]. Also Cole et al. measured F_3 for central Si+Au to be 0.55 ±0.15 [21] as compared to the minimum bias value from Table 3 of 0.66.

Table 3. Antiproton results from BNL-AGS

System	L^0_{HS}	$L^{2.48}_{SW}$	σ_{inel}	y	dn/dy	F_1	F_2	F_3	$\sigma/(A_1A_2)$	Ref.
p+Be	1.55	0.83	21	1.4	0.00038	2.0	1.00	0.86	15.2±4.8	[16]
p+Al	2.42	1.44	49	1.4	0.00047	2.0	1.00	0.85	14.5±4.5	[16]
p+Cu	3.30	2.06	93	1.4	0.00049	2.0	1.00	0.82	11.6±4.5	[16]
p+Au	4.86	2.92	208	1.4	0.00049	2.0	1.00	0.76	7.9±2.5	[16]
Si+Al	4.87	2.93	153	1.4	0.0100	2.0	0.35	0.82	11.6±2.5	[9]
Si+Au	7.31	4.41	390	1.4	0.0142	2.0	0.37	0.66	4.9±1.0	[9]
Au+Au	9.72	5.84	727	1.4	0.0150	2.0	0.40	0.53	1.2±0.3	[10]
p+Be	1.55	0.83	21	2.5	0.00074	3.5	1.00	1.00	60.4±6.0	[17]
p+Al	2.42	1.44	49	2.5	0.00069	3.5	1.00	1.00	43.8±5.2	[17]
p+Cu	3.30	2.06	93	2.5	0.00072	3.5	1.00	1.00	36.6±4.1	[17]
p+Pb	4.94	2.96	214	2.5	0.00050	3.5	1.00	1.00	18.1±1.9	[17]

Units and definitions are as in Table 1, except that all reduced cross sections have been multiplied by 10^4. Note that the data from [15] are at 19.2 GeV/c and the Au+Au is at 11.2 GeV/c.

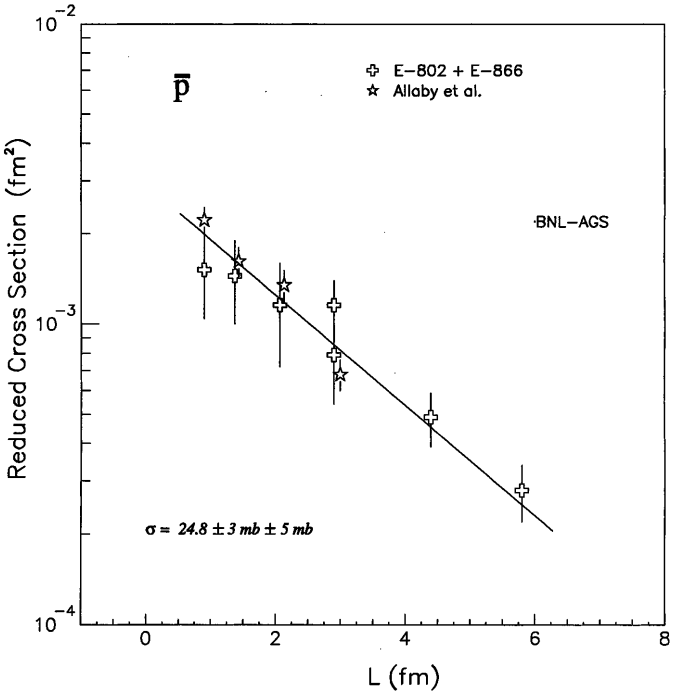

Fig. 3. Reduced cross sections for $\bar{p}$ measured at BNL-AGS. The Au+Au data obtained at 11.2 GeV are rescaled to 14.6 GeV by 2.4 while the data obtained at 19.2 GeV (Allaby et al.) are rescaled to 14..6 GeV by 1/2.7

All AGS data are presented in Fig. 3 along with p+A data obtained at 19.2 GeV/c at CERN. Data in the figure at beam momenta different from 14.6 GeV/c have been extrapolated to this beam momentum by means of the RQMD model. As can be seen from the figure, the reduced cross sections for $\bar{p}$ fall on a single exponential curve (χ^2/dof = 0.86) and the fitted value for the slope corresponds to $\sigma = 24.8 \pm 3 \pm 5$mb, where the external error corresponds to a systematic uncertainty of 50% on the F_3-values.

6 Discussion

The preceding analysis demonstrates that the reduced cross sections for $\bar{p}$ production in p+A and A_1+A_2 collisions follow exponentials as function of the characteristic length $L_{A_1A_2}$ calculated from a Glauber type absorption model, (4). As mentioned in the introduction and elaborated on below, it is not *a priori* justifiable to use the absorption model. The discussion presented here, deals with this question and further with what physics, if any, one can learn from the established systematics.

The fits to the exponentials may just reflect a general mass dependence, as given by (8), (11) and (12), i.e. the fits are not connected to the physics of the absorption model and may in this connection be taken as fortuitous.

The data presented here can in fact be fitted to other functional mass dependences, e.g. the SPS $\bar{p}$ follow to a similar accuracy the power law expression

$$\sigma(A_1 + A_2 \to \bar{p}) \propto (A_1 \cdot A_2)^{\alpha} \qquad (13)$$

with α=0.78±0.02.

The connection between the power law dependence and the Glauber-type absorption description has been discussed in some detail by Capella et al. [6], and it may be concluded from their work that the power of 0.78 found here makes a Glauber approach very doubtful. The empirical systematics, however, are very compelling and a brief examination of the physics conditions that must necessarily be fulfilled if a Glauber absorption model should be applicable is therefore presented.

The simplest condition of the absorption model (see the beginning of Sect. 2) is that particle X is a rarely produced particle, because the model does not allow multiple production. The very small p+p production cross sections for $\bar{p}$ and $\bar{\Lambda}$ [19] shows that this condition is well fulfilled at AGS and SPS energies.

In order for the concept of absorption to be realistic, the particle X must be produced within the nuclear volume and afterwards traverse part of it, in other words, the formation time should be small compared to the nuclear

linear dimension. For hard processes the formation time may be estimated by $\tau \approx 0.2/\Delta E$ in fm/c and the energy in GeV, which for production of a $p, \bar{p}$ pair in the nuclear rest system is $\approx$ 1fm/c as compared to ≈ 0.6 fm/c for J/Ψ. The hard processes then fulfil the condition on formation time, but at the AGS and SPS energies these processes are dominated by first collisions and are hence not evenly distributed through the nuclear volume, but peaked at the contact surfaces (see e.g [1,2,22]).

There may be other mechanisms than elementary hard collisions that are important for the production of $\bar{p}$ in heavy ion collisions, namely excitation of heavy resonances and the formation of di-strings or colour ropes (see e.g. [1, 2,22] and references cited there). In fact such "enhancement" mechanisms dominate the production cross sections in the RQMD model. The formation times after the creation of the intermediate excitation are short, 1-1.5 fm/c in the nuclear system, so the antibaryon is formed well within the nuclear volume and undergoes absorption on its way out. The various mechanisms may well conspire to produce a nearly evenly distributed set of formation locations as required for the validity of the absorption model.

The absorption model of (4) relates the production cross section to the elementary N+N (nucleon+nucleon) processes, in which the "enhancement" mechanisms invoked above, do not come into play. The absorption model, deals with elementary collisions between nucleons in heavy ion collisions, but not with the "enhancement" processes used by e.g. the RQMD model. Even if the absorption model is not valid for the processes studied here, the validity of (4) for the (A_1,A_2) dependence may come about if the "enhancement" mechanisms are proportional (or roughly proportional) to $A_1 \cdot A_2$. In that case (4) contains the right ingredients, but the cross sections are not related to the elementary N+N cross sections. The good fits to the power law pointed out above supports the idea that extra mechanisms may be nearly proportional to $A_1 \cdot A_2$.

If this proposition is accepted, the observed exponential slopes represent effective absorptions and not straightforward absorptions. The $\bar{p}$ absorption cross sections of 21 to 25 mb are much smaller than the free $p + \bar{p}$ annihilation cross sections (see e.g. [23,24]). This may then reflect a combination of "enhanced" production and absorption, and should not necessarily be interpreted as a quenching of the elementary absorption mechanisms. The small effective absorption found in the $\bar{\Lambda}$ case then does not represent the absence of elementary absorption processes, such as $\bar{\Lambda}+\pi \rightarrow K+\bar{N}$, but rather a combination of absorption and enhanced production, that here happens to combine to an almost vanishing effective absorption.

In summary, the reduced cross sections for antiproton and antilambda production in proton-nucleus and nucleus-nucleus minimum bias collisions follow the mass dependence predicted by a simple Glauber type absorption model. The model is strictly speaking not applicable, and the agreement between data and model may be fortuitous or may come about because the contributing production mechanisms are nearly proportional to $A_1 \cdot A_2$. The global mass dependence demonstrated certainly provides a rather stringent test for the various microscopic models in common use, e.g. RQMD, VENUS [25] and ARC [26].

The authors acknowledge the help of Aa. Winther and J. Bondorf with the evaluation of the absorption lengths $L_{A_1+A_2}$.

References

1. H. Sorge et al., Phys. Lett. B **289**, 6 (1992)
2. A. Jahns et al., Nucl. Phys. A **566**, 483c (1994)
3. S.H. Kahana et al., Phys. Rev. C **47**, R1356 (1993)
4. M.C. Abreu et al., the NA50 Collaboration, Phys. Lett. B **410**, 327 (1997)
5. M.C. Abreu et al., the NA50 Collaboration, Phys. Lett. B **410**, 337 (1997)
6. A. Cappella et al., Phys. Lett. B **206**, 354 (1988); J.P. Blaizot and J.Y. Ollitrault, Phys. Lett. B **217**, 392 (1989)
7. C. Gerschel and J. Hüfner, Phys. Lett. B **207**, 253 (1988); C. Gerschel and J. Hüfner, Z. Phys. C **56**, 172 (1992)
8. H. Sorge, R. Mattiello, H. Stöcker and W. Greiner, Phys. Rev. Lett. **68**, 286 (1992) and references therein
9. T. Abbott et al., the E802 Collaboration, Phys. Lett. B **271**, 447 (1991)
10. L. Ahle et al., the E802 Collaboration, Nucl. Phys. A **610**, 139c (1996)
11. T. Alber et al., the NA35 Collaboration, Phys. Lett. B **366**, 56(1996)
12. S.V. Afanasiev et al., the NA49 Collaboration, Nucl. Phys. A **610**, 188c (1996)
13. I.G. Bearden et al., the NA44 Collaboration, Phys. Rev. C **57**, 431 (1998)
14. I.G. Bearden et al., the NA44 Collaboration, Phys. Lett. B **388**, 31 (1996); M. Kaneta et al., the NA44 Collaboration, Nucl. Phys. A **638**, 419c (1998)
15. C. Borman et al., the NA49 Collaboration, J. Phys. G **23**, 1817 (1997)
16. T. Abbott et al., the E802 Collaboration, Phys. Rev. C **47**, R1351 (1993)
17. J.V. Allaby et al., CERN 70-12, 1970 (unpublished)
18. G.S.F. Stephans et al., the E802 Collaboration, Nucl. Phys. A **566**, 269c (1993)
19. A. Wroblewski, in *Proceedings of the Int. Symp. on Multiparticle Dynamics, Kayserberg 1977*; A. Wroblewski, Acta Phys. Pol. B **15**, 75 (1984)
20. M.J. Bennett et al., the E878 Collaboration, Phys. Rev. C **56**, 1521 (1997); T.A. Armstrong et al., the E864 Collaboration, nucl-ex/9709005 v2 (1997)
21. B.A. Cole et al., the E802 Collaboration, Nucl. Phys. A **590**, 196c (1995)
22. A. Jahns et al., Zeitschrift f. Physik, A **341**, 243 (1992); Phys. Rev. Lett., **68**, 2895(1992); Phys. Lett., B **308**, 1993 (1993)
23. V. Flaminio et al., CERN-HERA 8-01, 1984 (unpublished)
24. S. Gavin et al., Phys. Lett. B **234**, 175 (1990)
25. K. Werner, Z. Phys. C **42**, 85 (1989)
26. S. Kahana et al., Phys. Rev. C **47**, R1356 (1993), and references therein